UNIVERSAL WISER
PUBLISHER

A New Viscosity Constitutive Model for Generalized Newtonian Fluids Using Theory of Micropolar Continuum

Muhammad Sabeel Khan
Department of Mathematics, Sukkur Institute of Business Administration University, Sukkur 65200, Sindh, Pakistan
Email: drmsabeel@gmail.com

Abstract: In this paper, a new viscosity constitutive relation for the analysis of generalized Newtonian fluids is presented and analyzed. The theory of micropolar continuum is considered for the derivation of constitutive relations where the kinematics at the macroscopic level leads to incorporate the micro-rotational effects in existing rheology of Carreau-Yasuda model. It provides a more realistic approach to analyze the flow behavior of generalized Newtonian fluids. To the best of the author's knowledge such generalization of the existing rheology of Carreau-Yasuda is not present in literature. In order to show the effects of micro-rotations on the viscosity of generalized fluids, different computational experiments are performed using finite volume method (FVM). The method is implemented and validated for accuracy by comparison with existing literature in the limiting case through graphs and tables and a good agreement is achieved. It is observed that with the increase of micro-rotations the shear thinning phenomena slower down whereas the shear thickening is enhanced. Moreover, the effects of various model parameters on horizontal and vertical velocities as well as on boundary layer thickness are shown through graphs and contour plots It is worth mentioning that the proposed constitutive model can be utilized to analyze the generalized Newtonian fluids and has wider applications in blood rheology.
***Keywords*:** Generalized Newtonian fluid, Carreau-Yasuda model, Cross model, power law model, micropolar, finite volume method (FVM), shear rate dependent viscosity

1. Introduction

So far the shear rate dependent viscosity models [1–6] present in literature for the analysis of generalized Newtonian fluid (GNF) consider only shear rate dependence in classical continuum context. Whereas the GNF models with suspended particles behave as non-classical models so the theories like micropolar continuum best suits to analyze their behavior. Eringen [7] presented the micropolar theory of fluids considering independent micro-rotations of the fluid particles as additional vector field along with translational velocity field independent of fluid motions and rotations. Micropolar theory allows six degrees of freedom including micro-rotations as well as translations. Eringen [8] modified the constitutive relations for blood rheology by considering human blood as deformable suspension. Since Navier-Stokes equations are unable to model the non-Newtonian fluids like blood, ketchup and polymers with suspended particles, rotating independently irrespective of fluid's motion or rotation. Fluids having such microstructures with independent rotations of particles are termed as micropolar fluids. To model such behavior of fluids, a theory was needed which accounts for geometry, deformation and intrinsic motion of individual fluid particles which was given by Eringen [7, 9, 10].

The Micropolar theory also known as the Cosserat Continuum theory (CCT) initially proposed by Cosserat brothers [11] is a non-classical higher order theory which incorporates six degrees of freedom by considering three independent self-centered micro rotations along with three translational motions and thus provides a deeper information at micro level which affects overall behavior of flow at macro level. Cosserat theory includes internal couple stresses which lead to asymmetry of the Cauchy stress tensor and thus provides a more realistic approach towards mathematical modelling of such phenomena. Micropolar model is actually a generalization of Navier-Stokes model which introduced an additional vector field of angular velocity influenced by rotation of particles. Several experiments show that the micropolar theory better represents the behavior of GNF like polymers, liquid crystals and blood than the classical theory.

DOI: https://doi.org/10.37256/cm.132020152

In the context of classical continuum theory, some popular classical models [1, 4, 6] for GNFs as well as in some non-classical models [12–15] are present in literature and are listed below.

1.1 The power law model [1]

Modified Ostwald-deWaele relation for shear stress τ is given as

$$\tau = m\left|\dot{\gamma}\right|^{n-1}\dot{\gamma} \tag{1}$$

Where $\mu_{eff}\left(\dot{\gamma}\right) = m\left|\dot{\gamma}\right|^{n-1}$ is effective viscosity, m is model parameter and n is the power index and

$$\left|\dot{\gamma}\right| = \sqrt{\frac{1}{2}\left(\left(\frac{\partial u}{\partial x}\right)^2 + \left(\frac{\partial v}{\partial y}\right)^2 + \left(\frac{\partial u}{\partial y} + \frac{\partial v}{\partial x}\right)^2\right)} \tag{2}$$

1.2 The Carreau-Yasuda model [6]

The Carreau-Yasuda model for the viscosity in the context of classical as well as non-classical theories discussed in literature so far is given by

$$\mu_{eff}(\dot{\gamma}) = \left[\mu_\infty + (\mu_0 - \mu_\infty)\{1 + \lambda(|\dot{\gamma}|)^a\}^{\frac{n-1}{a}}\right] \tag{3}$$

where $\dot{\gamma}$ is as in subsection 1.1 above.

1.3 The Cross model [4]

The effective viscosity for Cross model for shear thinning fluids is given as

$$\mu_{eff}\left(\dot{\gamma}\right) = \left[\mu_\infty + \frac{\left(\mu_0 - \mu_\infty\right)}{\left(1 + \lambda\left(\left|\dot{\gamma}\right|\right)^n\right)}\right] \tag{4}$$

where μ_0 is the viscosity at zero shear rate, μ_∞ is the viscosity at the infinite shear rate, λ is dimensionless relaxation time and n is the power index.

These models only consider the translational motion of the particle while defining viscosity constitutive relation and do not incorporate the micro-rotations. However, for a complete picture in the theoretical description of constitutive relation for viscosity it is important to consider micro-rotations of the fluid particles.

In this study, a generalized constitutive relation for the viscosity of GNFs is presented. In particular, the power law model [1], Cross model [4] and Carreau-Yasuda model [6] are reconsidered in the context of micropolar theory [8] for the first time in literature. The new constitutive relation for viscosity is used with the micropolar continuum model for the flow analysis through lid-driven cavity. Different numerical experiments are performed to analyze the flow behavior using this constitutive relation.

2. New viscosity constitutive model for generalized Newtonian fluids

A generalized Newtonian fluid is a non-Newtonian fluid for which shear stress is a function of shear rate satisfying the following rheological equation.

$$\boldsymbol{\tau} = \mu_{eff}\left(\dot{\gamma}\right)\dot{\gamma} \tag{5}$$

Where τ is the shear stress, $\dot{\gamma}$ is the shear rate and $\mu_{eff}\left(\dot{\gamma}\right)$ is called the effective viscosity function.

The constitutive equations for GNF presented in equation (5) has been used by many researchers in the different context, that is in the analysis of GNF for both the classical and non-classical case but the theory of the non-classical

continuum has not been completely used to derive this relation. In this context this section presents a new constitutive equation for the effective viscosity $\mu_{eff}(\dot{\gamma})$ of GNF with the incorporation of the micropolar rotations of the particle at the continuum scale. This new constitutive relation completely considers the kinematics of the micropolar theory and as a result incorporates the effect of micro-rotation at the continuum scale into the existing theory for GNF viscosity. The new constitutive relation for non-classical case is derived by considering the non-classical shear rate tensor.

$$\dot{\boldsymbol{\gamma}}_{mic} = \dot{\gamma}_{ij} - E_{ijk}\phi_k \tag{6}$$

The absolute is computed as $|\dot{\gamma}_{mic}| = \sqrt{I_2}$, where I_2 is the second invariant of the strain tensor and is calculated as $I_2 = \frac{1}{2}tr(\mathbf{A}^2) = \frac{1}{2}\Sigma\Sigma A_{ij}A_{ji}$, and the tensor $\mathbf{A}$ is the strain tensorin $\mathbf{A} = \varepsilon_{ij} - E_{ijk}\phi_k$, the context of micropolar continuum. After some calculations, the following relation is achieved

$$|\dot{\gamma}_{mic}| = \sqrt{\frac{1}{2}\left(\left(\frac{\partial u}{\partial x}\right)^2 + \left(\frac{\partial v}{\partial y}\right)^2 + \frac{1}{2}\left(\frac{\partial u}{\partial y} + \frac{\partial v}{\partial x} - \phi_3{}^2\right)^2\right)} \tag{7}$$

The new generalized relation for the effective viscosity for the Carreau-Yasuda model is thus given as

$$\mu_{eff}(\dot{\gamma}) = \left[\mu_\infty + (\mu_0 - \mu_\infty)\left\{1 + \lambda\left(|\dot{\boldsymbol{\gamma}}_{mic}|\right)^a\right\}^{\frac{n-1}{a}}\right] \tag{8}$$

It can be noted that in the absence of micro-rotations ϕ_3 this model reduces to classical Carreau-Yasuda model [6] (and as mentioned in subsection 1.2 above) and furthermore, with a = 2 it reduces to the commonly used Carreau model [5]. Some of the applications of such models are described in the papers [20-24].

3. Physical model problem

Consider a two dimensional steady, laminar and incompressible state of the micropolar generalized Newtonian fluid in in a square lid driven cavity with boundary conditions as shown in Figure 1 below.

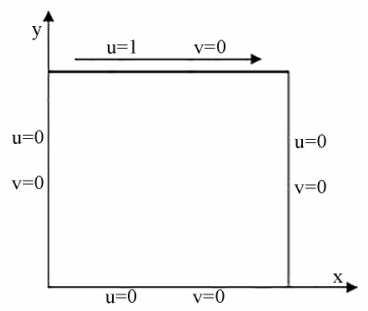

Figure 1. Geometry and boundary conditions of the problem

The fluid flow is derived by a constant velocity U_{lid} at the top boundary and is governed by following [7, 8, 11] set of PDEs.

$$\frac{D\rho}{Dt} = -\rho(\nabla.\mathbf{V}) \tag{9}$$

$$\rho\frac{D\mathbf{V}}{Dt} = \nabla\boldsymbol{\tau} + \rho f \tag{10}$$

$$\rho I \frac{D\mathbf{\Phi}}{Dt} = \nabla.\mathbf{C} + \rho g + \mathbf{E} \cdot \boldsymbol{\tau} \tag{11}$$

Where **V**, Φ, f, $\boldsymbol{\tau}$ and **C** are velocity vector, angular velocity of rotation, body force, stress tensor and couple stress tensor, respectively. Here the components of tensors $\boldsymbol{\tau}$ and **C** are to be determined [9, 10] by the following constitutive relations, respectively

$$\tau_{ij} = -P\delta_{ij} + \left(2\mu + \kappa\right) D_{ij} + \kappa E_{ijk}\left(w_k - \Phi_k\right) \tag{12}$$

$$C_{ij} = \alpha \Phi_{k,k}\delta_{ij} + \beta \Phi_{i,j} + \gamma \Phi_{j,i} \tag{13}$$

Where **V**, Φ, f, $\boldsymbol{\tau}$ and **C** are velocity vector, angular velocity of rotation, body force, stress tensor and couple stress tensor, respectively. Here the components of tensors $\boldsymbol{\tau}$ and **C** are to be determined [9, 10] by the following constitutive relations, respectively

Where $D_{ij} = \varepsilon_{ij} = \frac{1}{2}\left(u_{i,j} + u_{j,i}\right)$ (14)

and $w_{ij} = \frac{1}{2}\left(u_{j,i} - u_{i,j}\right)$ (15)

Above P, μ, κ, **D** and **w** are pressured, viscosity, curvature, strain rate tensor and vorticity, respectively. Whereas α, β and γ are coefficients of angular viscosities. In a two-dimensional dimensionless setting the governing equations (9-11) takes the following forms

$$\frac{\partial u}{\partial x} + \frac{\partial v}{\partial y} = 0 \tag{16}$$

$$\frac{\partial\left(u^2\right)}{\partial x} + \frac{\partial\left(uv\right)}{\partial y} = \frac{1+K}{\mathrm{Re}}\left(\frac{\partial^2 u}{\partial x^2} + \frac{\partial^2 u}{\partial y^2}\right) - \frac{\partial P}{\partial x} + \frac{K}{\mathrm{Re}}\frac{\partial \phi}{\partial y} \tag{17}$$

$$\frac{\partial\left(v^2\right)}{\partial x} + \frac{\partial\left(uv\right)}{\partial y} = \frac{1+K}{\mathrm{Re}}\left(\frac{\partial^2 v}{\partial x^2} + \frac{\partial^2 v}{\partial y^2}\right) - \frac{\partial P}{\partial y} - \frac{K}{\mathrm{Re}}\frac{\partial \phi}{\partial x} \tag{18}$$

$$\frac{\partial\left(u\phi\right)}{\partial x} + \frac{\partial\left(v\phi\right)}{\partial y} = \frac{1}{\mathrm{Re}}\left(1 + \frac{K}{2}\right)\left(\frac{\partial^2 \phi}{\partial x^2} + \frac{\partial^2 \phi}{\partial y^2}\right) - \frac{2K\phi}{\mathrm{Re}} + \frac{K}{\mathrm{Re}}\left(\frac{\partial v}{\partial x} - \frac{\partial u}{\partial y}\right) \tag{19}$$

Where $\Phi = \left(\phi_1, \phi_2, \phi_3\right) = \left(0, 0, \phi\right), \mathrm{Re} = \frac{U_{lid} L}{\mu_0}$ and $U_{lid} = u_{\max}$.

4. Solution methodology and validation of computer code

To solve the system of partial differential equations (16-19) finite volume method (FVM) is used to discretize the system and the problem is implemented in MATLAB. The pressure-velocity coupling is resolved by using uniform staggered mesh. In this respect, a semi-implicit method for pressure linked equations algorithm with a hybrid scheme given by Versteege and Malalasekara [16] is implemented over a 100 × 100 grid to investigate parametric effects of α, n and λ on the flow. The convergence criteria was set using a tolerance of 10^{-5}. For details of finite volume discretization of PDEs and

implementation methodology the reader is referred to the book by Versteege and Malalasekara [16]. The implemented program is tested for the case of Newtonian fluid up to Re = 3200 and set $n = 1$ and assume viscosity to be constant as $\mu = \mu_0$. The results are found in good agreement with the results presented in the literature. In Table 1, a comparison of *u*-velocities along a vertical line is made with the results given by Ghia et al [18] and good agreement is found. The results for the case of Newtonian flow are also shown in Table 2 where a comparison is made for the *v*- velocities with its existing counterpart in literature and also a very agreement are achieved. These simulation results thereby validate the accuracy of the implementation of the finite volume method for this problem and the results achieved further for the problem in consideration.

Table 1. *u*- velocities along vertical line through Geometric Center of cavity

Grid point	Y	Re							
		100		400		1000		3200	
		Ghia et al. [18]	Present	Ghia et al. [18]	Present	Ghia et al. [18]	Present	Ghia et al. [18]	Present
1	0.0000	0.00000	0.0000	0.0000	0.0000	0.0000	0.0000	0.0000	0.0000
8	0.0547	-0.03717	-0.0367	-0.08186	-0.0818	-0.18109	-0.1814	-0.32407	-0.3240
9	0.0625	-0.04192	-0.0414	-0.09266	-0.0918	-0.18109	-0.2015	0.35344	0.3534
10	0.0703	-0.04775	-0.0460	-0.10338	-0.1080	-0.22220	-0.2210	-0.37827	-0.3781
14	0.1016	-0.06434	-0.0637	-0.14612	-0.1514	-0.29730	-0.2898	-0.41933	-0.4191
23	0.1719	-0.10150	-0.1011	-0.24299	-0.2479	-0.38289	-0.3827	-0.34323	-0.3431
37	0.2813	-0.15662	-0.1570	-0.32726	-0.3269	-0.27805	-0.2778	-0.24427	-0.2443
59	0.4531	-0.21090	-0.2129	-0.17119	-0.1685	-0.10648	-0.1056	-0.86636	-0.8653
65	0.5000	-0.20581	-0.2061	-0.11477	-0.1131	-0.06080	-0.0588	-0.04272	-0.0428
80	0.6172	-0.13641	-0.1375	0.02135	0.0211	0.05702	-0.0581	0.07156	0.0708
95	0.7344	0.00332	0.0029	0.16256	0.1587	0.18719	0.1814	0.19791	0.1971
110	0.8516	0.23151	0.2294	0.29093	0.2867	0.33304	0.3312	0.34682	0.3468
123	0.9531	0.68717	0.6792	0.55892	0.5545	0.46604	0.4566	0.46101	0.4562
124	0.9609	0.73722	0.7297	0.61756	0.6088	0.51117	0.5112	0.46547	0.4651
125	0.9688	0.78871	0.7978	0.68439	0.6815	0.57492	0.5744	0.48296	0.4829
126	0.9766	0.84123	0.8387	0.75837	0.7519	0.65928	0.6519	0.53236	0.5331
129	1.0000	1.00000	1.0000	1.00000	1.0000	1.00000	1.0000	1.00000	1.0000

Table 2. *v*- velocities along horizontal line through Geometric Center of cavity

Grid point	X	Re							
		100		400		1000		3200	
		Ghia et al. [18]	Present	Ghia et al. [18]	Present	Ghia et al. [18]	Present	Ghia et al. [18]	Present
1	0.0000	0.00000	0.0000	0.00000	0.0000	0.00000	0.0000	0.00000	0.0000
9	0.0625	0.09233	0.0926	0.18360	0.1834	0.27485	0.2747	0.39560	0.3956
10	0.0703	0.10091	0.1012	0.19713	0.1970	0.29012	0.2901	0.40917	0.4092
11	0.0781	0.10890	0.1093	0.20920	0.2082	0.30353	0.3031	0.41906	0.4190
13	0.0938	0.12317	0.1237	0.22965	0.2310	0.32627	0.3261	0.42768	0.4275
21	0.1563	0.16077	0.1606	0.28124	0.2831	0.37095	0.3708	0.37119	0.3717
30	0.2266	0.17507	0.1774	0.30203	0.3028	0.33075	0.3304	0.29030	0.2903
31	0.2344	0.17527	0.1776	0.30174	0.3035	0.32235	0.3225	0.28188	0.2818
65	0.5000	0.05454	0.05506	0.05186	0.0515	0.02526	0.0251	0.00999	0.0098
104	0.8047	-0.24533	-0.2459	-0.38598	-0.3891	-0.31966	-0.3196	-0.31184	-0.3117
111	0.8594	-0.22445	-0.2165	-0.44993	-0.4476	-0.42665	-0.4264	-0.37401	-0.3741
117	0.9063	-0.16914	-0.1650	-0.23827	-0.2376	-0.51550	-0.5150	-0.44307	-0.4430
122	0.9453	0.10313	-0.1038	-0.22847	-0.2274	-0.39188	-0.3914	-0.54053	-0.5404
123	0.9531	0.08864	-0.0876	-0.19254	-0.1912	-0.33714	-0.3370	-0.52357	-0.5237
124	0.9609	-0.07391	-0.0739	-0.15663	-0.1569	-0.27669	-0.2760	-0.47425	-0.4741
125	0.9688	-0.05906	-0.0591	-0.12146	-0.1214	-0.21388	-0.2138	-0.39017	-0.3902
129	0.0000	0.0000	0.0000	0.00000	0.0000	0.00000	0.0000	0.00000	0.0000

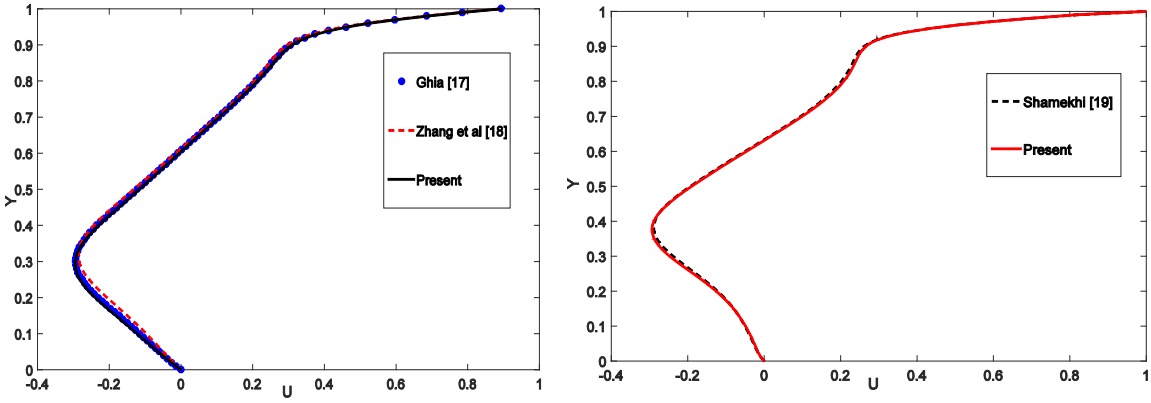

(a) (b)

Figure 1. Midline u-velocity comparison for Re=400 for (a) Newtonian and (b) non-Newtonian case

In Figure 1 a comparison for midline *u*- velocity for the Newtonian and Non-Newtonian cases are shown. The results for the Newtonian case taken by Ghia et al [17] and Zhang et al [18] are compared with the one by present method and found in good agreement. This shows the accuracy of implemented computer code. Moreover, the obtained results are also compared for the case of classical generalised Newtonian Carreau-Yasuda fluid model with the numerical results presented by Shamekhi et al [19] using the PIM meshfree method. It is found that the obtained results are in excellent agreement.

5. Results and discussion

In this section the results obtained by utilizing the derived viscosity constitutive relation are presented. For this purpose, three different models for micropolar generalized Newtonian fluids i.e. power law, Carreau-Yasuda and Cross models are analyzed numerically using FVM. The analysis performed is presented below.

5.1 Analysis of power law model in conjunction with new theory

The newly developed constitutive relation for shear rate viscosity is implemented for flow in a lid driven cavity. To analyze the effects of model parameters *m*, *n* and *K* viscosity curves are plotted. It can be seen in Figure 2(a) that viscosity at higher shear rate reduces as *n* decreases which results in reduction of boundary layer thickness near $y = 1$ as a decrease in viscosity leads to lowering the boundary layer thickness when $n < 1$. The comparison for viscosity graphs for both classical and micropolar cases is also given in Figure 2(a) and 2(b) for shear thinning and thickening cases which demonstrates that the viscosity for highest shear rate in micropolar case is different than classical model. Thus, the presence of micro-rotations affects the boundary layer thickness. An increase in *m*, shifts the transition region of viscosity curve to lower shear rate. The effects of parameter in the presence of micro-rotational parameter *K* on viscosity for both shear thinning and shear thickening cases are shown in Figure 2(b) and 2 (c). For larger *m*, viscosity at highest shear rate is smaller which causes a reduction in boundary layer thickness as shown in Figure 2. Midline horizontal and vertical velocities for both classical and micropolar cases with different values of power law index *n* are shown in Figure (3-4). It can be seen from Figure 3 that as *n* decreases, the velocities deviates from Newtonian to power law region for shear thinning case whereas when $n > 1$, the velocities deviates from Newtonian to shear thickening region as shown in Figure 4.

The effects on micro-rotational velocities for different values of power law index *n* and model parameter *m* for both shear thinning and shear thickening cases are shown in Figure 5(a-c). Self-centered micro-rotations of particles cause change in viscosity and that is shown through contour plots with micro-rotational parameter *K* in Figure 6 and 7. The difference in viscous behavior of fluid in presence and absence of these micro-rotations for both shear thinning and shear thickening cases is seen which concludes the importance of inclusion of these micro-rotations for viscosity measurements.

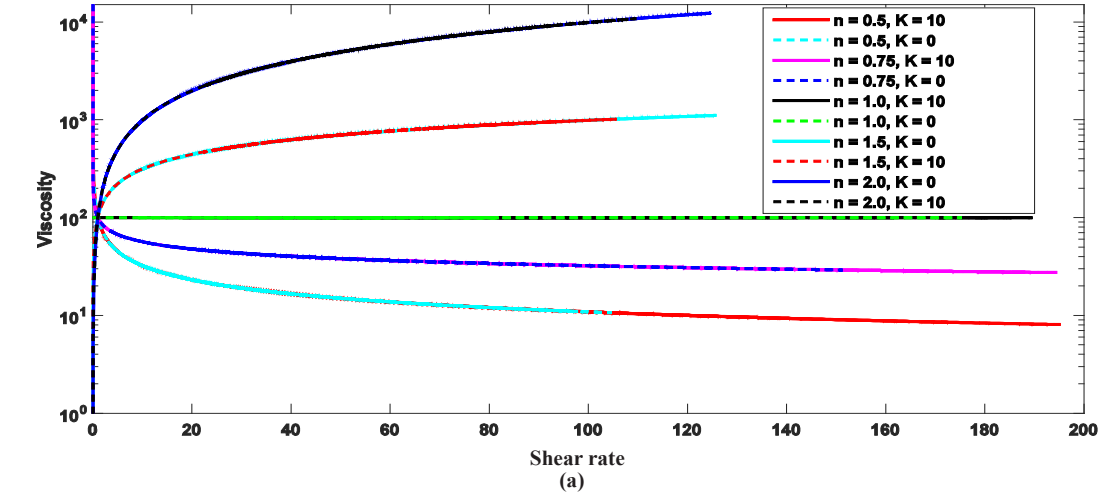

(a)

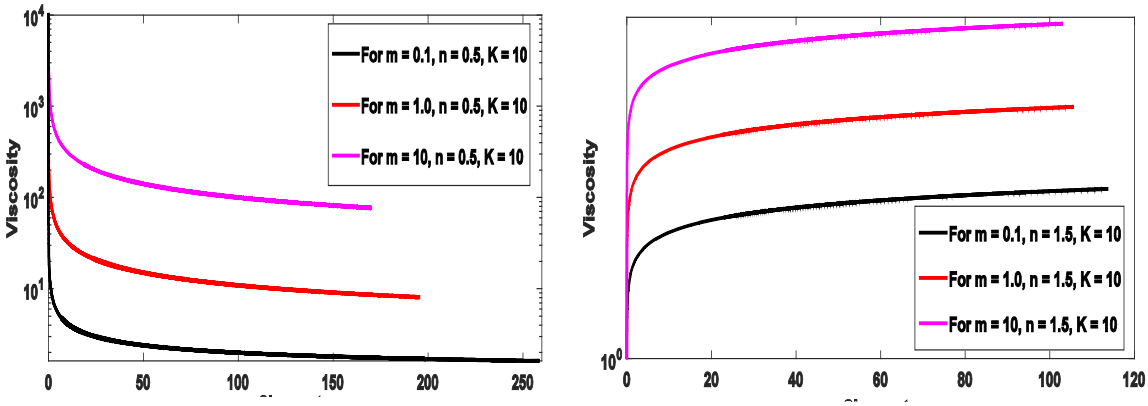

(b) (c)

Figure 2. Shear rate versus viscosity graphs for (a) different values of *n* with and without micropolar rotations (b) varying *m* for shear thinning case (c) varying *m* for shear thickening case

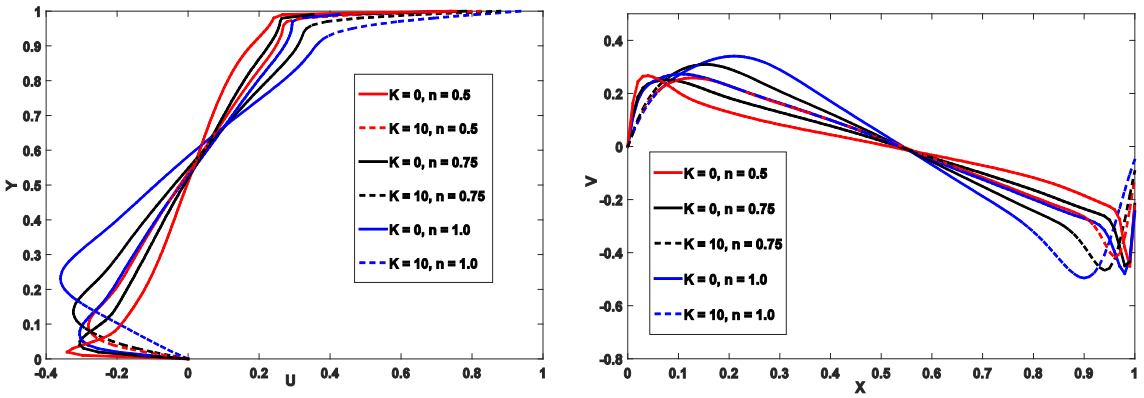

(a) (b)

Figure 3. Variations of *n* and *K* for midline velocities for shear thinning and Newtonian fluids (a) *u* velocity (b) *v* velocity

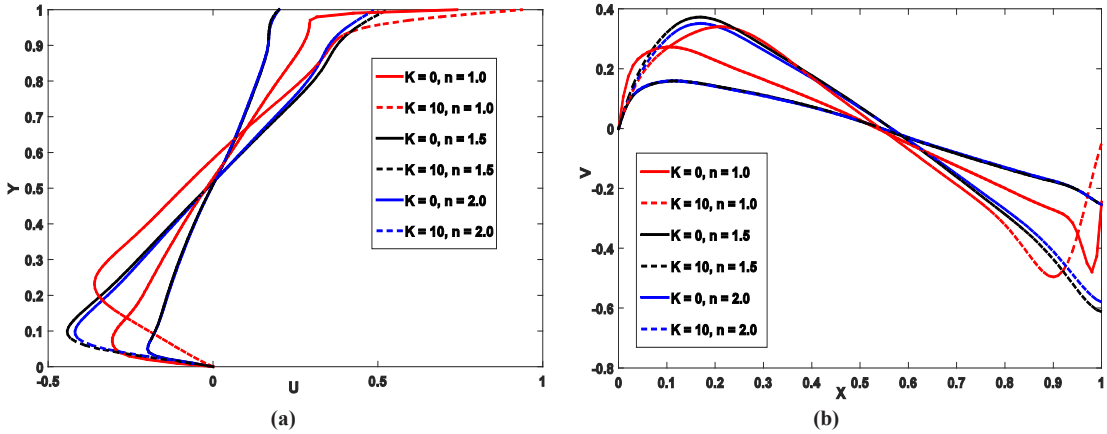

(a) (b)

Figure 4. Variations of *n* and *K* for midline velocities for Newtonian and shear thickening fluids (a) *u* velocity (b) *v* velocity

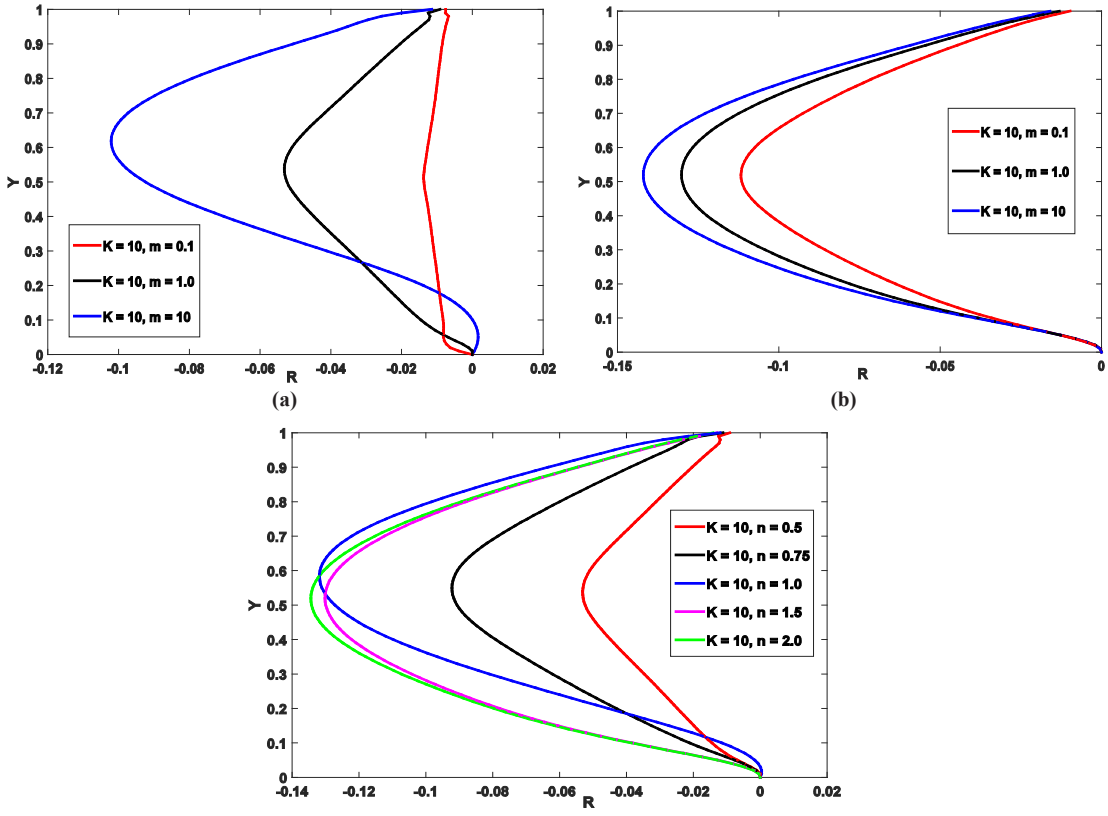

(a) (b)

(c)

Figure 5. Variations of micro-rotational velocity with (a) varying *m* for shear thinning (b)varying *m* for shear thickening (c) varying *n* for shear thinning, Newtonian and shear thickening fluids

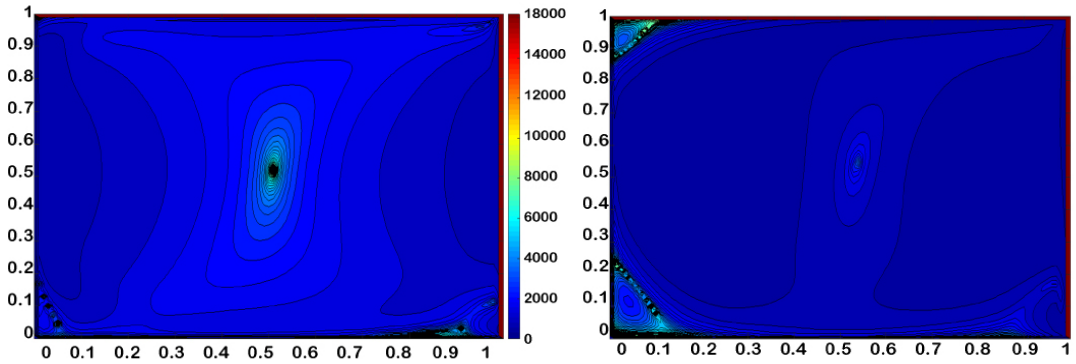

(a) (b)

Figure 6. Viscosity contours for shear thinning fluid when *n* = 0.5

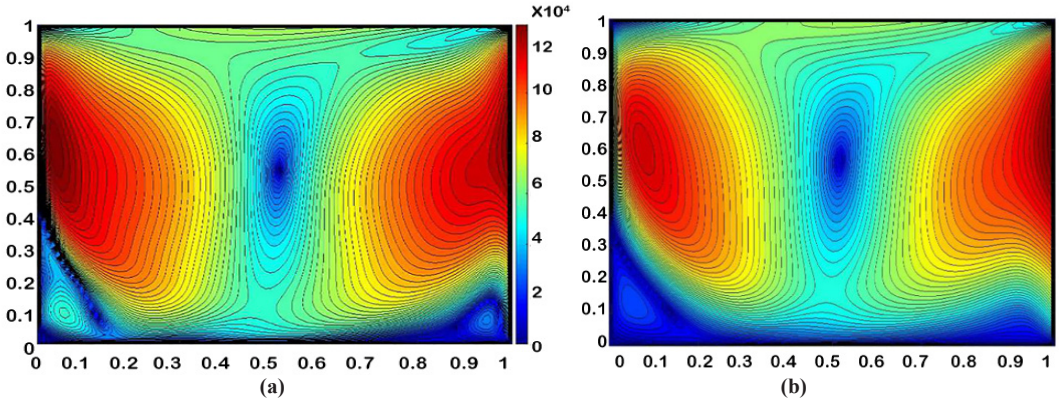

Figure 7. Viscosity contours for shear thickening fluid when n = 1.5. (a) Classical power law viscosity when K = 0 (b) Micropolar power law viscosity when K = 10

5.2 Analysis of Carreau-Yasuda model in conjunction with new theory

Here the effects of different parameters are investigated using the newly developed model on the flow behavior in a lid driven cavity. For this purpose a 100 × 100 grid is used with following parametric values $\lambda = 1$, $\alpha = 1$, $K = 10$ and $\mu = 100\mu_\infty$. in the case of present model. To understand the viscosity curves given in Figure (8-10), consider near lid region at $x = 0.5$, when constant horizontal velocity $u = 1$ is applied and shear rate is relatively higher; instead of lid moving in positive direction, we can think conversely that fluid moves in negative x- direction with constant velocity beneath the fixed lid where a boundary layer is formed. A boundary layer thickness is affected by fluid viscosity; it is reduced as the viscosity decreases. Figure (8-10) explain the reason of the change in boundary layer thickness due to variation of parameters n, λ and α. Viscosity at higher shear rate reduces as n decreases which results in reduction of boundary layer thickness near $y = 1$ for shear thinning case as shown in Figure 8(a). The comparison for viscosity graphs for both classical and micropolar cases is also given in Figure 8(a) and 8(b) for shear thinning and thickening cases which demonstrates that the viscosity for highest shear rate is different than classical model and thus, the viscosity cannot be calculated correctly by neglecting micro-rotations. Thus, the inclusion of micro-rotations results in better prediction of viscosity measurements. For larger λ, viscosity at highest shear rate is smaller which causes in a reduction in boundary layer thickness as shown in Figure 9 (a). An increase in λ shifts the transition region of viscosity curve to lower shear rate. The effects of micropolar rotations along with varying λ on viscosity curves are shown for both shear thinning and shear thickening cases in Figure 8. It can be seen in Figure 10(a) that for $a = 1$ and $a = 0.5$, boundary layer thickness is smaller whereas thickness is almost same for $0.5 \leq a \leq 10$. A decrease in a lowers the viscosity with changing the curve shape as shown in Figure 10(a-b) for both shear thinning and shear thickening cases. Figure 11(a-b) shows the effects of variations of n on u and v velocities; as n decreases, u and v deviate more from the Newtonian fluid region (at $n = 1$) because the slope of power law region in viscosity curve for smaller n is more different than (at $n = 1$). Similarly the effects of model parameters a, K, λ and n on rotational velocity are shown in Figure 12(a-d).

The effects of micro-rotational parameter K on viscosity are shown through contour plots for shear thinning when n = 0.5 for both classical and micropolar cases in Figure 13(a) and 13(b) respectively. It can be seen from these figures that if we include the micro-rotations, then the shear thinning phenomena will be slower and viscosity contours shows a different picture than classical model. For n =1 viscosity becomes constant and flow is Newtonian but for $n > 1$, the phenomena is shear thickening. The effects of K are shown for thickening case in Figure 14(a) and 14(b) for classical and micropolar cases and it can be observed that with the increasing values of micro-rotation parameter K the process of shear thickening will be enhanced.

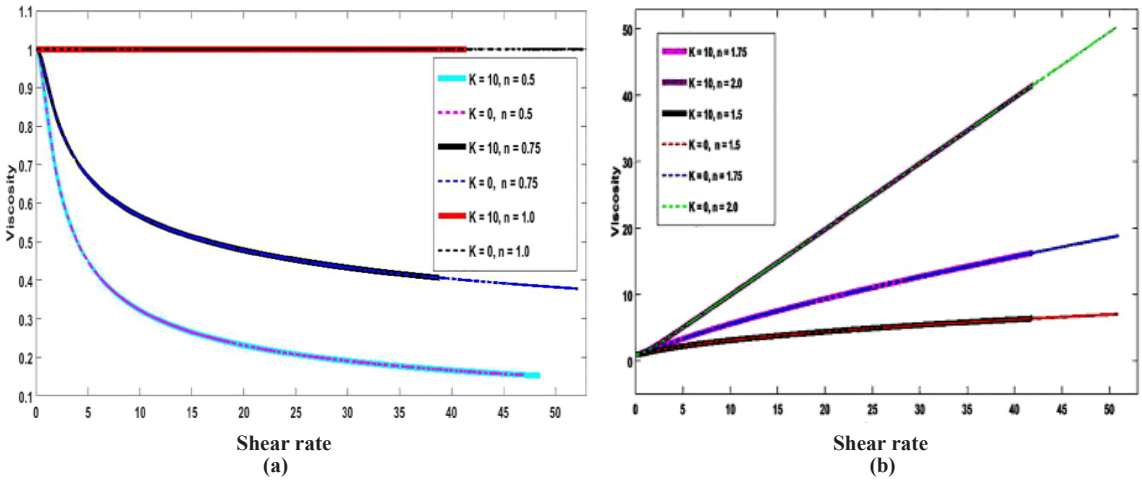

(a) (b)

Figure 8. Shear rate VS viscosity graphs for different values of *n* with and without micro-polar rotations for (a) shear thinning case (b) shear thickening case

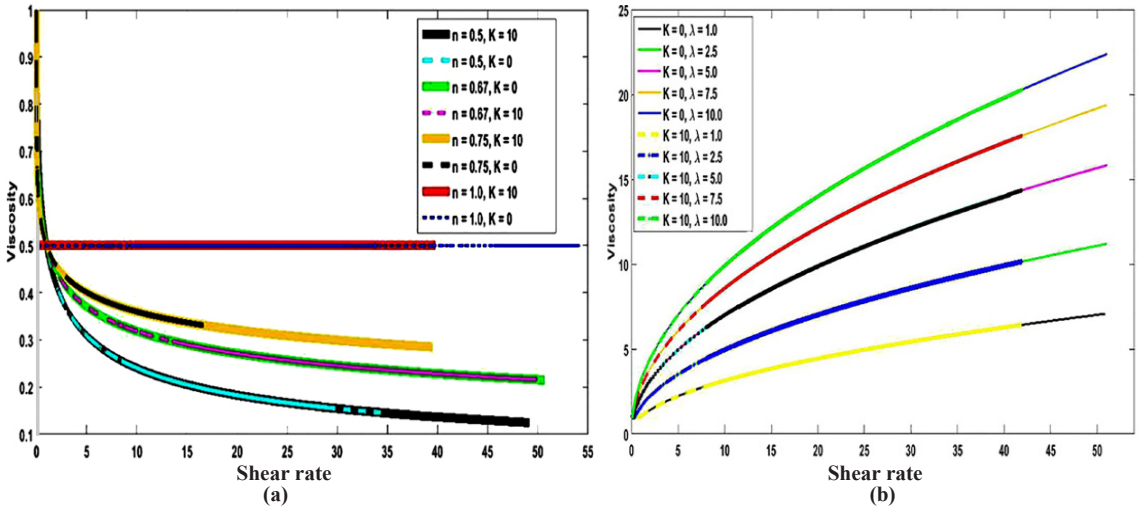

(a) (b)

Figure 9. Shear rate VS viscosity graphs for different values of λ with and without micro-polar rotations for (a) shear thinning case (b) shear thickening case

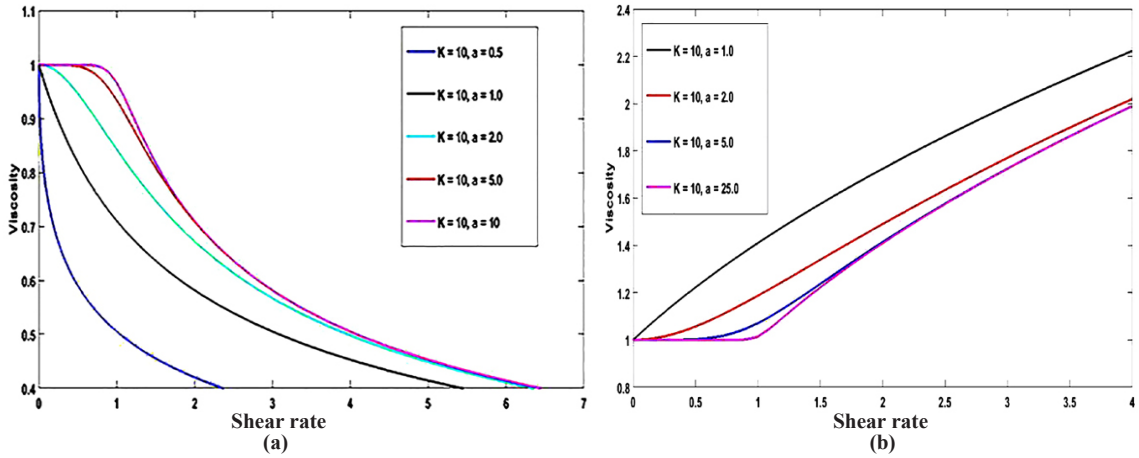

(a) (b)

Figure 10. Shear rate VS viscosity graphs for different values of model parameter *a* (a) shear thinning case (b) shear thickening case

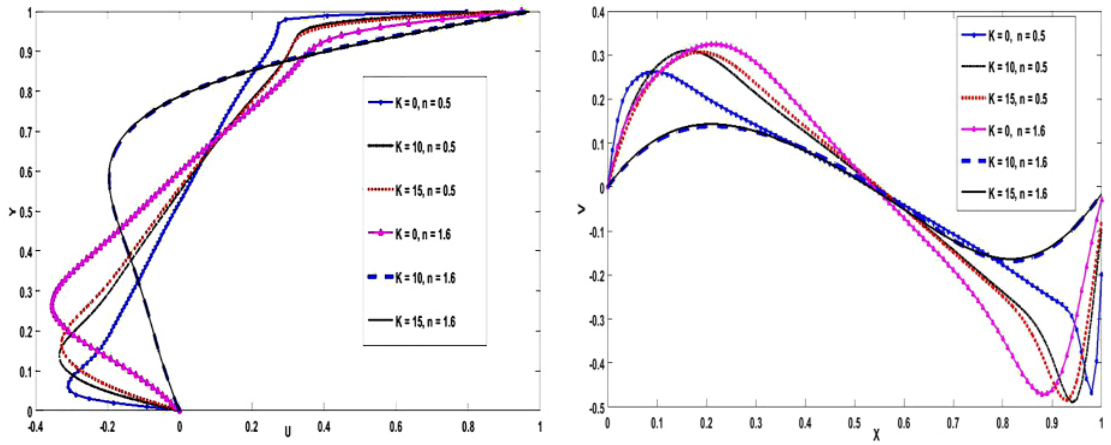

(a) (b)

Figure 11. Variations of *n* and *K* for midline velocities for shear thinning and shear thickening fluids with and without micro-polar rotations (a) *u* velocity (b) *v* velocity

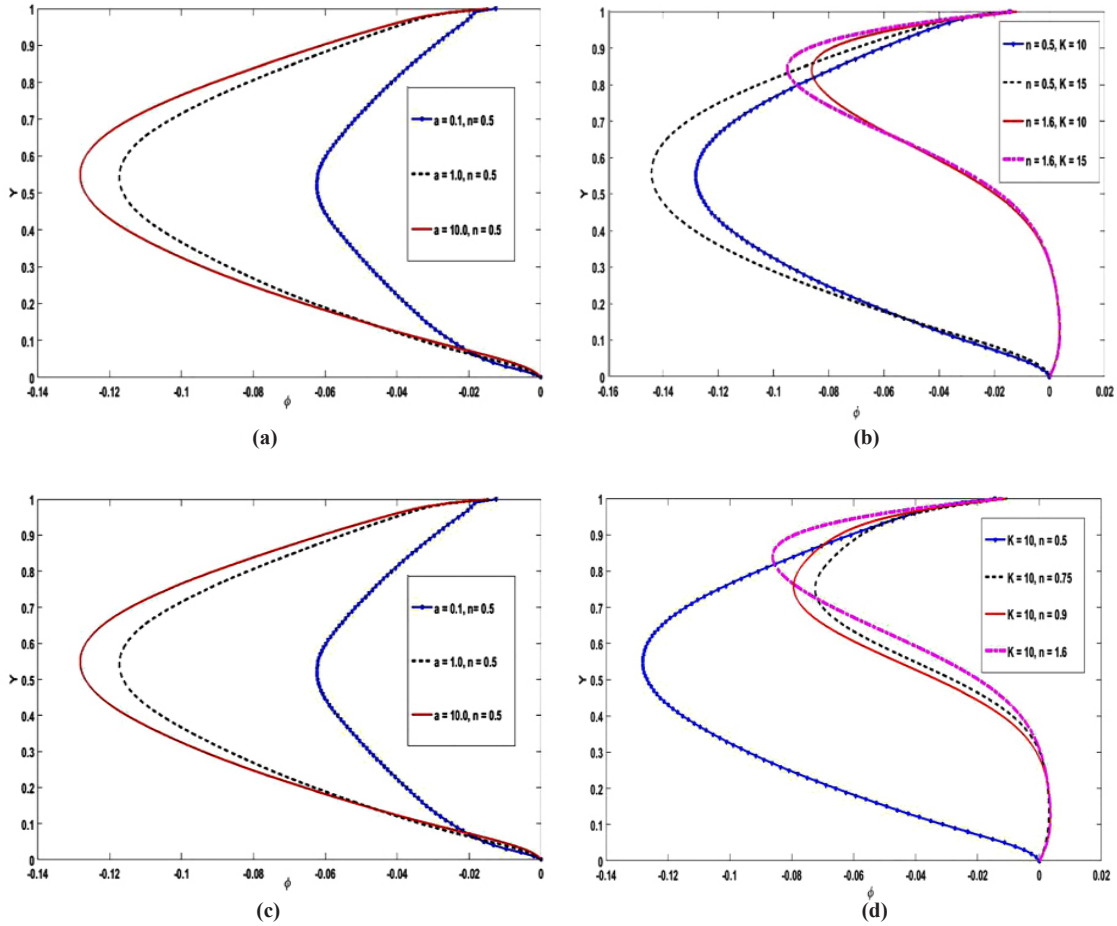

(a) (b)

(c) (d)

Figure 12. Variations of micro-rotational velocity with (a) varying *a* for shear thinning (b) varying micro-rotations parameter *K* (c) varying *λ* for shear thinning (d) varying *n*

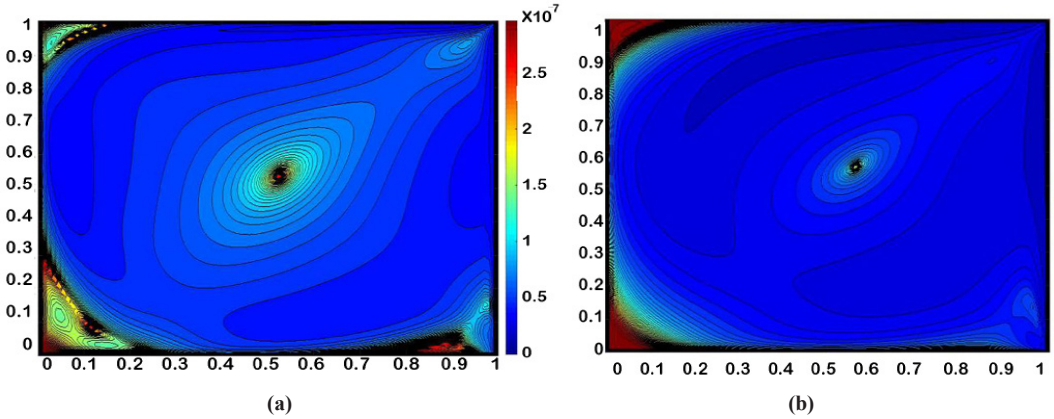

Figure 13. Viscosity contours for shear thinning fluid when n = 0.5, (a) Classical Carreau-Yasuda viscosity when K = 0 (b) Micropolar Carreau-Yasuda viscosity when K = 10

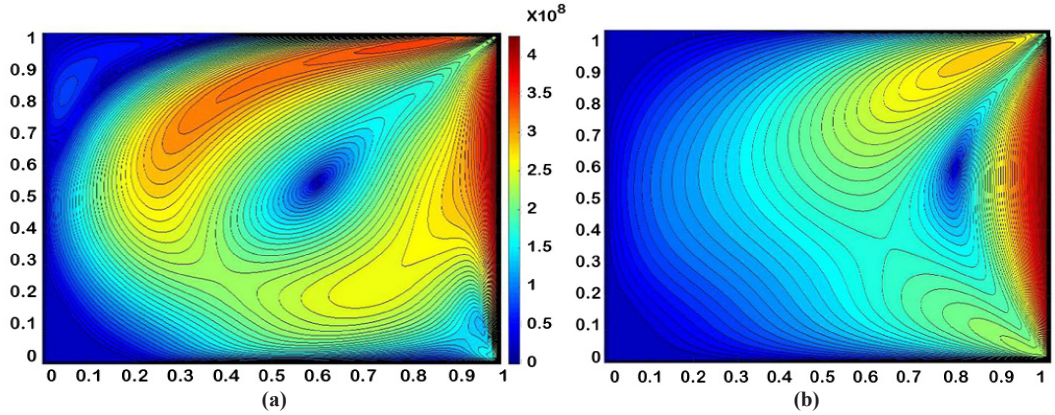

Figure 14. Viscosity contours for shear thickening fluid when n = 1.5, (a) Classical Carreau-Yasuda viscosity when K = 0 (b) Micropolar Carreau-Yasuda viscosity when K = 10

5.3 Analysis of cross model in conjunction with new theory

The effective viscosity for Cross fluid is also modified in for shear thinning fluids and this newly developed relation for viscosity is used for GNF flow in lid driven cavity. The effects of different model parameters K, λ and n on viscosity curves and thus on boundary layer thickness are analyzed. Figure 15 shows that a decrease in the value of power law index lowers the value of viscosity for the highest share rate and thus causes a reduction for boundary layer thickness.

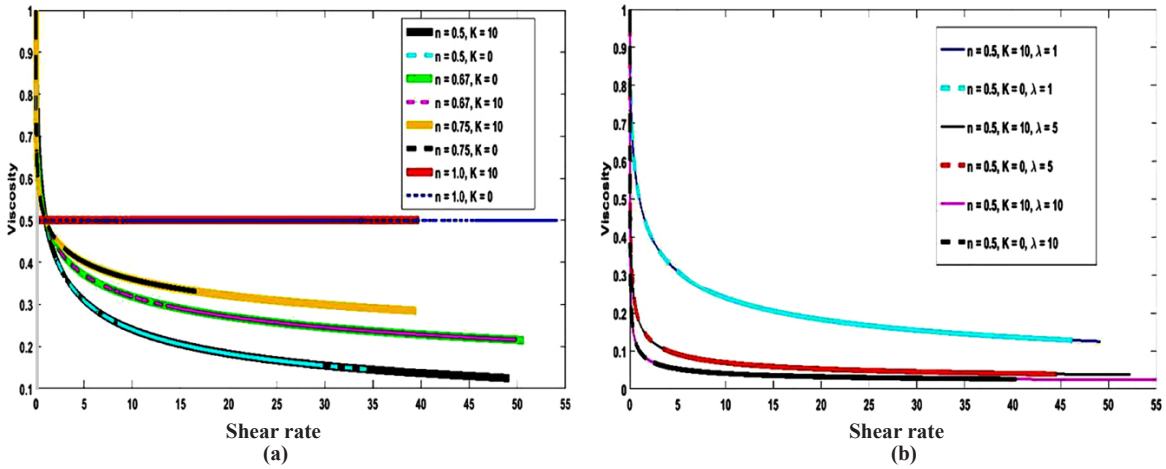

Figure 15. Shear rate VS viscosity graphs with and without micro-polar rotations for (a) differentvalues of n (b) varying values of λ

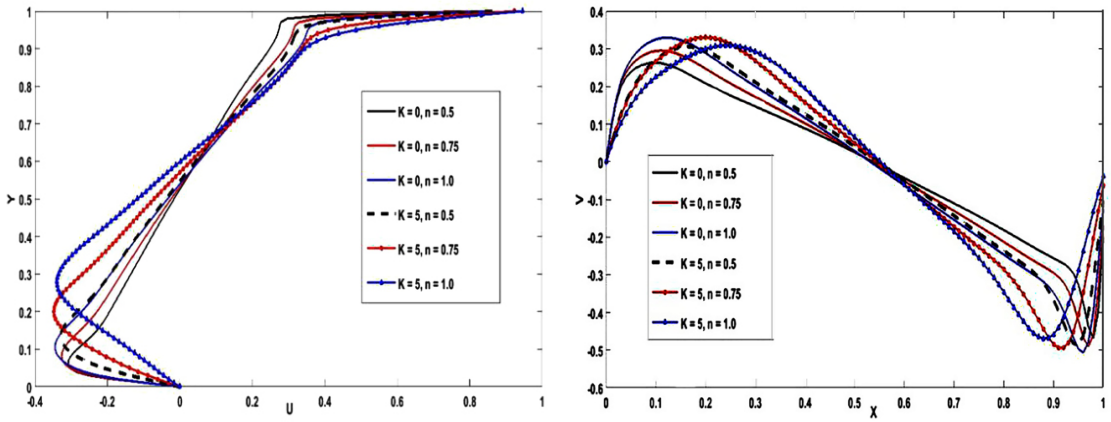

Figure 16. Variations of *n* for midline velocities for shear thinning fluids with and without micro-polar rotations (a) *u* velocity (b) *v* velocity

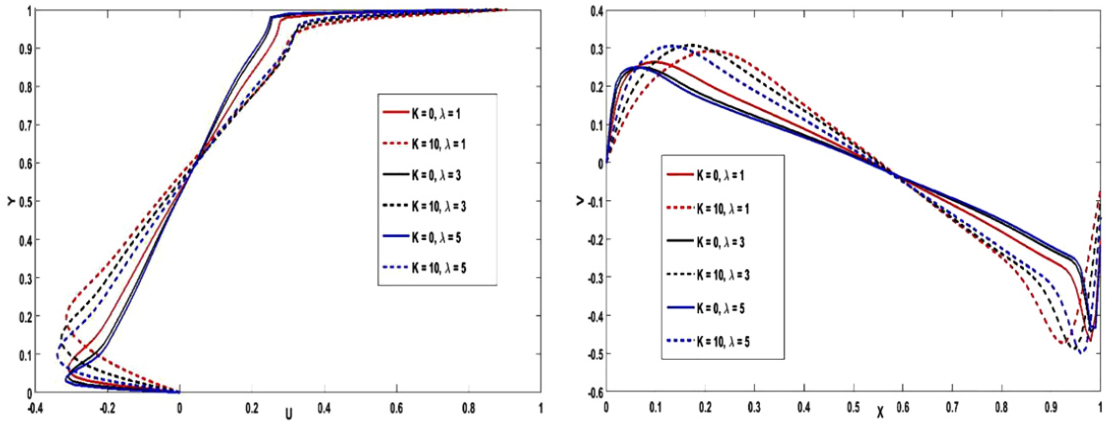

Figure 17. Variations of *n* and *K* for midline velocities for shear thinning fluids with varying *λ*

The effects of the micro-rotational parameter K on viscosity curves with varying values of for shear thinning are shown in Figure 15(a). It can also be observed that micro-rotations affect the viscosity at highest shear rates and thus a considerable change will occur on boundary layer thickness.

An increase in λ will cause the lowering of viscosity at highest shear rate and leads to reduction of boundary layer thickness which can be seen in Figure 15(b). Micro-rotations will also affect the viscosity value at highest shear rate shown in Figure 15(b). Midline horizontal and vertical velocities for different values of power law index are plotted for both classical and micropolar cases along $x = 0.5$ in Figure 16, respectively. It can be seen that as n decreases, u and v deviate more from the Newtonian fluid region because the slope of power law region in viscosity curve for smaller n is more different than at $n = 1$. It can also be observed in Figure 16 that the micropolar rotations will also affect the midline velocities and cause deviations. Figure 17 shows the deviations of midline velocities with varying values of λ and micro-rotations parameter K. In Figure 18, the effects of micropolar rotations K on shear rate dependent viscosity can be observed through contour plots which are drawn for $n = 0.75$. Figure 18(a) shows the viscosity contours when $K = 0$, in the absence of micro-rotations whereas Figure 18(b) is taken for $K = 5$. By comparing these two figures, it can be observed that micro-rotations slower down the shear thinning phenomena as micro-rotations slower down the translational motion of particles. An increase in the micro-rotations to a value of $K = 10$, reduce the shear thinning phenomena as shown in Figure 18(c). Thus, it is important to consider the micro-rotational motions of particles so that shear rate dependent viscosity can be calculated with a more realistic approach.

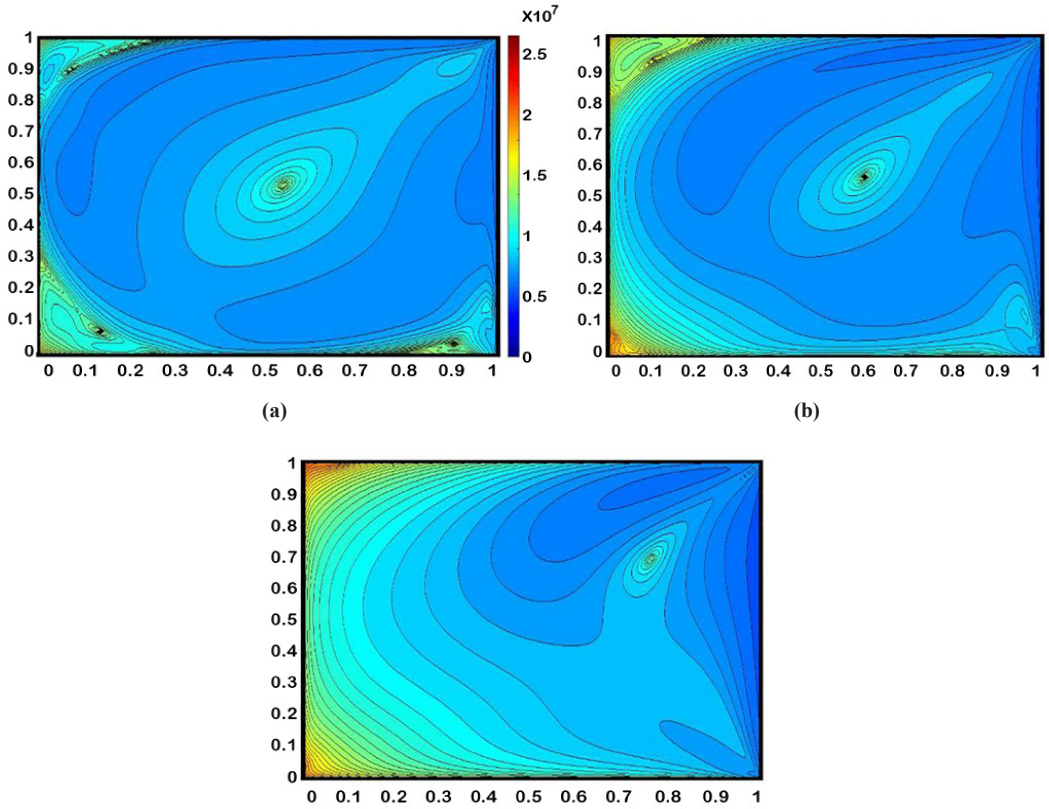

Figure 18. Viscosity contours for shear thinning fluid when $n = 0.75$ for (a) $K = 0$, (b) $K = 5$, (c) $K = 10$

6. Conclusion

A new non-classical constitutive equation for viscosity of generalized Newtonian fluids (GNF) is presented for the first time in literature. It is based on the kinematics of micropolar theory which considers self-centered micro-rotations as well as translations of the fluid particles and thus provides a more realistic approach towards the analysis of blood rheology in particular and GNF in general. Three different GNFs viscosity models are revisited using the new constitutive viscosity relation by FVM in the context of micropolar continuum and flow analysis in a lid driven cavity is carried out. The findings of this investigation are summarized as follows:

• Micro-rotations affect the viscosity at highest shear rates and thus the boundary layer thickness affected.

• The rate of change in the shapes of u and v velocities grows as parameter a decreases.

• As time relaxation parameter λ increases, it shifts the transition region of a viscosity curve to lower shear rate which leads to variations in horizontal and vertical velocities.

• For larger λ, viscosity is smaller which causes reduction in boundary layer thickness.

• Viscosity at higher shear rate reduces as n decreases which results in reduction of boundary layer thickness.

• An Increase in the micro-rotations slows down the shear thinning phenomena.

• The shear thickening process can be enhanced by increasing the micro-rotation parameter K.

References

[1] Ostwald W. Ueber die rechnerische darstellung des strukturgebietes der viskosität. *Kolloid-Zeitschrift*. 1929; 47(2): 176-87.

[2] Oldroyd JG. On the formulation of rheological equations of state. *Proc R Soc A Math Phys Eng Sci*. 1950; 200(1063): 523-41.

[3] Casson, N. A flow equation for pigment-oil suspensions of the printing ink type. *Rheol Disperse Syst*. 1959.

[4] Cross MM. Rheology of non-Newtonian fluids: A new flow equation for pseudoplastic systems. *J Colloid Sci*. 1965; 20(5): 417-37.

[5] Agassant J, Avenas P, Carreau PJ. *Polymer Processing Principles and Modeling*.
[6] Yasuda K, Armstrong RC, Cohen RE. Shear flow properties of concentrated solutions of linear and star branched polystyrenes. *Rheol Acta*. 1981; 20(2): 163-78.
[7] Eringen AC, Suhubi ES. Nonlinear theory of simple micro-elastic solids-I. *Int J Eng Sci*. 1964; 2(2): 189-203.
[8] Kang CK, Eringen AC. The effect of microstructure on the rheological properties of blood. *Bull Math Biol*. 1976; 38(2): 135-159.
[9] Eringen A.C. Theory of Micropolar Fluids. *Journal of Mathematics and Mechanics*. (16): 1-18.
[10] Eringen AC. Theory of Micropolar Elasticity. *In: Microcontinuum Field Theories*. New York, NY: Springer New York; 1999; 101-248.
[11] Cosserat E, Delphenich DH. *Theory of deformable bodies*. 1906.
[12] Rahman MM. *Effects of Higher Order Chemical Reaction on Micropolar Fluid Flow on a Power Law*. 2010; 88: 23-32.
[13] Sui J, Zhao P, Cheng Z, *et al*. *A novel investigation of a micropolar fluid characterized by nonlinear constitutive diffusion model in boundary layer flow and heat transfer*. 2017; 023105: 1-10.
[14] Atif SM, Hussain S, Sagheer M. *Numerical study of MHD micropolar carreau nanofluid in the presence of induced magnetic field*. 2018; 035219.
[15] Ellahi R, Rahman SU, Gulzar MM, *et al*. *A mathematical study of Non-Newtonian micropolar fluid in arterial blood flow through composite stenosis*. 2014; 1573(4): 1567-1573.
[16] Versteeg HK, Malalasekera W. *An introduction to computational fluid dynamics: the finite volume method*. Pearson Education Ltd; 2007. 503.
[17] Ghia U, Ghia KN, Shin CT. High-Re solutions for incompressible flow using the Navier-Stokes equations and a multigrid method. *J Comput Phys*. 1982; 48(3): 387-411.
[18] Liu GR, Zhang GY, Gu YT, *et al*. A meshfree radial point interpolation method (RPIM) for three-dimensional solids. *Comput Mech*. 2005; 36(6): 421-30.
[19] Shamekhi A, Aliabadi A. *Non-Newtonian Lid-driven Cavity Flow Simulation by Mesh Free Method*. 2009; 11(3): 67-72.
[20] Numerical investigation for peristaltic flow of Carreau-Yasuda magneto-nanofluid with modified Darcy and radiation. *Journal of Thermal Analysis and Calorimetry.* 2019; 137: 1359-1367.
[21] Hydromagnetic peristalsis of water based nanofluids with temperature dependent viscosity: A comparative study. *Mol. Liquids*. 2017; 234: 324-329.
[22] Entropy generation analysis for peristaltic motion of Carreau-Yasuda nanomaterial. *Physica Scripta*. 2019.
[23] Carreau. Rheological equations from molecular network theories. *Journal of Rheology*. 1972; 16: 99-127.
[24] Numerical study for peristalsis of Carreau-Yasuda nanomaterial with convective and zero mass flux condition. *Results in Physics*. 2018; 8: 1168-1177.
[25] Double diffusive unsteady convective micropolar flow past a vertical porous plate moving through binary mixture using modified Boussinesq approximation. *Ain Shams Engineering Journal*. 7(2): 755-765.
[26] Melting heat and mass transfer in stagnation point micropolar fluid flow of temperature dependent fluid viscosity and thermal conductivity at constant vortex viscosity. *Journal of the Egyptian Mathematical Society*. 25(1): 79-85.
[27] New similarity solution of micropolar fluid flow problem over an uhspr in the presence of quartic kind of autocatalytic chemical reaction. *Frontiers in Heat and Mass Transfer*. 8.
[28] Exploration of the significance of autocatalytic chemical eeaction and cattaneo-christov heat flux on the dynamics of a micropolar fluid. *Journal of Applied and Computational Mechanics*. 6(1): 77-89.